Materials Advances

ROYAL SOCIETY OF CHEMISTRY

PAPER

View Article Online
View Journal | View Issue

Cite this: *Mater. Adv.*, 2025, **6**, 2371

Anthocyanin-sensitized Cu-doped TiO_2 nanoparticles for efficient and sustainable DSSCs

Kamal Prajapat,†[a] Ujjwal Mahajan,†[a] Mahesh Dhonde,*[a] Kirti Sahu,[b] P. Sakthivel,[c] Shweta Vyas[d] and P. M. Shirage[e]

The growing demand for efficient and sustainable energy solutions has driven significant interest in dye-sensitized solar cells (DSSCs) utilizing natural dyes. However, enhancing their performance and long-term stability remains a major challenge. This study aims to address this gap by synthesizing Cu-doped TiO_2 nanoparticles (NPs) and investigating their application as photoanodes in DSSCs to improve energy conversion efficiency. Using a cost-effective and facile co-precipitation method, Cu-doped TiO_2 photoanodes were prepared with varying Cu concentrations (0.025 M, 0.05 M, 0.075 M, and 0.1 M) and tested with anthocyanin dye extracted from rose petals. The performance of pure and Cu-doped photoanodes in a DSSC configuration was evaluated using various physical, optical and electrical tools. The photovoltaic and charge transport characteristics were assessed using current density–voltage (*J–V*) measurements, incident photon-to-electron conversion efficiency (IPCE), and electrochemical impedance spectroscopy (EIS). Among the tested samples, the 0.075 M Cu-doped TiO_2 photoanode exhibited superior performance, outperforming both pristine TiO_2 and other doping concentrations. When integrated with anthocyanin dye, the DSSC featuring 0.075 M Cu-doped TiO_2 demonstrated a notable enhancement in photocurrent density, increasing from 5.8 to 7.6 mA cm^{-2}, while the power conversion efficiency (PCE) improved from 1.53% to 2.61%. This enhancement is attributed to the improved light-harvesting capability of Cu-doped TiO_2, along with reduced electron transport resistance and increased recombination resistance, as confirmed by EIS analysis. These findings highlight the potential of Cu-doped TiO_2 photoanodes as an effective alternative to pure TiO_2 nanostructures for advanced photovoltaic applications. Beyond DSSCs, these enhanced photoanodes hold promise for broader applications, including photocatalysis for wastewater treatment and photo-sensing technologies, further expanding their role in sustainable energy and environmental solutions.

Received 31st December 2024,
Accepted 12th March 2025

DOI: 10.1039/d4ma01297f

rsc.li/materials-advances

1. Introduction

The growing global demand for sustainable energy sources has driven significant advancements in photovoltaic (PV) technology, particularly in the development of third-generation solar cells. Among these, DSSCs have garnered considerable attention due to their cost-effective fabrication, high efficiency, and potential for diverse applications.[1] DSSCs offer several advantages over traditional and other emerging PV technologies, including simpler and more economical production processes.[2] These cells have demonstrated power conversion efficiencies (PCEs) exceeding 14%, with the added potential for integration into various applications, making them a promising alternative for renewable energy generation.[3] A critical component of DSSCs is the sensitizer, which plays a key role in determining the cell's overall performance. While ruthenium (Ru) bipyridyl compounds are commonly used as sensitizers due to their stability and high efficiency, they present several drawbacks, such as high cost, complex synthesis, and the use of toxic materials.[4,5] These limitations have prompted researchers to explore alternative, more sustainable sensitizers, such as natural dyes extracted from flower leaves, seeds, bark, and fruits. Natural dyes contain plant pigments like anthocyanins, carotenoids, chlorophyll, and flavonoids, which can effectively absorb light and facilitate electron injection into the conduction band of TiO_2.[6]

[a] *Department of Physics, Medi-Caps University, Indore 453331, Madhya Pradesh, India. E-mail: maheshdhonde86@gmail.com*
[b] *Department of Physics, Prime Minister College of Excellence, Government Holkar (Model Autonomous) Science College, Indore 452001, Madhya Pradesh, India*
[c] *Centre for Materials Science, Department of Science and Humanities, Faculty of Engineering, Karpagam Academy of Higher Education, Coimbatore – 641021, Tamil Nadu, India*
[d] *Department of Pure and Applied Chemistry, University of Kota, Kota 324005, Rajasthan, India*
[e] *Department of Metallurgy Engineering and Materials Science, Indian Institute of Technology, Indore 453552, M.P., India*
† These authors contributed equally to the work.

Anthocyanins, for instance, are flavonoid pigments found in rose petals that have gained attention as natural sensitizers in DSSCs due to their wide absorption range in the visible spectrum and strong attachment to TiO_2 molecules through carboxyl groups.[7] Additionally, the high antioxidant concentration in anthocyanins provides a protective effect by scavenging free radicals generated during photoelectrode photoexcitation.[8] Despite these advantages, natural dye-based DSSCs still face challenges in achieving efficiency levels comparable to conventional silicon solar cells, limiting their broader application. To improve the PCE of natural dye-sensitized DSSCs, it is essential to optimize photoanode design to enhance dye loading, sunlight scattering, charge carrier transport, and minimize recombination losses.[9,10]

Metal oxides such as TiO_2, ZnO, SnO_2, and Nb_2O_5 with mesoporous nanostructures are commonly used as photoanodes in DSSCs, where they play a crucial role in light absorption, charge separation, and electron transport.[11–13] Recent efforts to enhance the performance of DSSC photoanodes have focused on doping metal oxides with transition metals. Doping introduces localized energy states within the TiO_2 bandgap, enabling the absorption of a broader range of solar radiation, particularly in the visible spectrum, which is typically underutilized in undoped TiO_2-based devices.[14–16]

Among various dopants, copper (Cu) has emerged as a particularly promising candidate for improving the photoelectrochemical properties of TiO_2-based photoanodes in DSSCs. Incorporating Cu ions into the TiO_2 lattice alters the electronic structure, promoting efficient charge carrier separation and transport, thus enhancing the overall photovoltaic performance.[11,17–19] Furthermore, Cu doping reduces recombination losses at the photoanode/electrolyte interface, leading to higher DSSC efficiency.[20] The co-precipitation method is widely used for synthesizing Cu-doped TiO_2 NPs due to its simplicity, scalability, and ability to control doping concentration and particle morphology. This approach ensures uniform dispersion of Cu ions within the TiO_2 lattice, maximizing the beneficial effects on DSSC performance.[21]

Several studies have demonstrated the effectiveness of Cu-doped TiO_2 NPs synthesized by the co-precipitation method in DSSC applications. For example, Raguram *et al.* reported enhanced charge transport and reduced recombination rates in DSSCs utilizing Cu-doped TiO_2 NPs synthesized *via* co-precipitation.[22] Similarly, Prabavathy *et al.* achieved a PCE of 2.32% using Ca-doped TiO_2 nanostructures sensitized with anthocyanins.[23] Recent work by Omri *et al.* also reported significant improvements in electrical conductivity upon Cu doping in TiO_2 compared to undoped counterparts, highlighting the potential for these nanostructures in optoelectronic devices.[24] Despite these advancements, challenges remain in optimizing synthesis parameters, controlling dopant distribution, and ensuring the long-term stability of Cu-doped TiO_2 NPs in DSSCs. In a recent report, Abhishek *et al.* examines the use of Beta vulgaris dye in DSSCs to study Fe-doped TiO_2 nanorod photoanodes ($Ti_{1-x}Fe_xO_2$, x = 0–0.1), which were developed on FTO electrodes using a hydrothermal process.[25] The findings revealed that incorporating 5 at% Fe increased the maximum photocurrent density from 80 to 129.758 mA cm^{-2} and doubled the PCE from 0.26% to 0.52%. This enhancement is attributed to improved charge injection and separation. The study suggests that $Ti_{1-x}Fe_xO_2$ photoanodes could effectively replace pure TiO_2 in photovoltaic applications and also hold potential for photocatalytic and photosensor uses.

In this research, we explore the use of Cu-doped TiO_2 as a photoanode in DSSCs with natural anthocyanin dye. While traditional DSSCs using synthetic dyes like N719 often achieve efficiencies beyond 10% due to their strong light absorption and stability, natural dyes like anthocyanin have inherent limitations that result in lower efficiency. Our Cu-doped TiO_2 DSSC achieved an efficiency of 2.61%, which, although lower than synthetic dye-based devices, highlights the potential of Cu doping to enhance performance. The introduction of Cu into the TiO_2 structure offers several advantages over pure TiO_2. It improves light absorption by narrowing the bandgap, enhances charge separation by reducing recombination losses, and increases electrical conductivity by creating oxygen vacancies. These modifications lead to improved photocurrent density and overall device performance despite the limitations of the natural dye. Moreover, Cu-doped TiO_2 enhances chemical stability, reducing the degradation of the dye and prolonging DSSC efficiency over time. While the efficiency of our DSSC does not reach the levels of Ru-dye-based devices, Cu doping presents a promising strategy to enhance the performance of eco-friendly, cost-effective DSSCs using natural sensitizers.

This study is unique because it focuses on improving eco-friendly and cost-effective DSSCs using a natural dye rather than synthetic alternatives. The findings demonstrate that Cu doping can significantly enhance the performance of natural dye-based DSSCs, making them a promising alternative for sustainable solar energy applications. To the best of our knowledge, this is the first report of combining Cu-doped TiO_2 NPs with anthocyanins for DSSC applications. Our results highlight the promising potential of natural DSSCs and open new avenues for innovative nanostructured photoanodes in PV technologies to meet small-scale energy needs more effectively.

2. Experimental details

2.1. Materials

Titanium tetra-isopropoxide (TTIP), copper nitrate trihydrate ($Cu(NO_3)_2{\cdot}3H_2O$), ethanol, sodium hydroxide (NaOH), glacial acetic acid, and citric acid (all from Sigma Aldrich). Anthocyanin dye was extracted from fresh rose petals. Iodide electrolytes and FTO glass were sourced from Solaronix.

2.2. Preparation of pure and Cu-doped TiO_2 NPs

Undoped and Cu-doped TiO_2 NPs were synthesized using a controlled co-precipitation method as discussed in our previous report.[26] The synthesis of undoped TiO_2 began with the preparation of a titanium precursor solution by adding 11.84 mL of TTIP (1 M) dropwise into 40 mL of ethanol under

continuous stirring for one hour. This controlled addition prevented rapid hydrolysis and ensured proper dispersion. A sodium hydroxide (NaOH) solution (2 M in ethanol) was then introduced to facilitate hydrolysis and precipitation while maintaining constant magnetic stirring for an additional two hours at 30 °C. The resulting precipitate was collected through filtration and thoroughly washed with distilled water and ethanol to remove impurities.[26] The dried precipitate was subjected to calcination at 450 °C for 30 minutes to enhance crystallinity, yielding pure TiO_2 nanoparticles.

For Cu-doped TiO_2 nanoparticles, two separate solutions were initially prepared. Solution A contained 11.84 mL of TTIP mixed with 40 mL of ethanol and stirred for one hour. Solution B consisted of copper nitrate trihydrate ($Cu(NO_3)_2{\cdot}3H_2O$) dissolved in deionized water at concentrations ranging from 0.025 M to 0.1 M, with pH adjusted to 10 using NaOH. After mixing for 30 minutes, solution B was added dropwise to solution A, followed by continuous stirring for 15 hours to promote uniform doping. The resulting suspension was centrifuged, and the solid phase was washed multiple times with ethanol to eliminate unreacted precursors. The purified precipitate was then vacuum-dried at 100 °C for one hour and annealed at 450 °C for 30 minutes to obtain Cu-doped TiO_2 nanoparticles. This method successfully produced well-crystallized and homogeneously doped TiO_2 nanostructures, offering enhanced material properties suitable for various applications.

2.3. Anthocyanin dye extraction

To prepare the dye, 10 gm of fresh rose petals were placed in a container with 30 mL of citric acid. The container was kept in the dark for a day to prevent light from affecting the solvent's effectiveness. After this period, the same extract was reused to extract more dye from another batch of fresh rose petals, increasing the dye's concentration.[23] The mixture was centrifuged to eliminate solid particles and then filtered. The resulting liquid dye was then used for sensitizing the photoanodes.

2.4. DSSC assemmbly

A DSSC device was fabricated by assembling prepared pure and Cu-doped TiO_2 photoanodes combined with a platinum (Pt) counter electrode (CE). The photo-anodes were immersed in the anthocyanin dye solution for the whole night for dye loading.[27] The DSSC was constructed by stacking the photoanode and the Pt CE on top of one other, while leaving space for external circuit connections. Two droplets of the prepared electrolyte were introduced between the photoanode and the CE.[28] The assembly was held together using a pair of binder clips to secure the device in place for testing delicately.

2.5. Characterization

Powder XRD analysis was carried out on a Bruker D8 Advance X-ray diffractometer equipped with monochromatic Cu Kα radiation. The surface morphology was analyzed using FE-SEM (JEOL JSM-7600F) and TEM (JEM-2010, JEOL). Optical properties were measured with a PerkinElmer Lambda25 UV-vis spectrophotometer. Raman spectra were recorded using an HJY micro-Raman spectrometer with a 633 nm He–Ne laser. The photovoltaic performance of DSSCs was tested under standard simulated 1.5G solar radiation (Oriel Sol 3A, Newport, model 94063A), and IPCE was determined using a Bentham PVE300 quantum efficiency system.

3. Result and discussion

3.1. Powder XRD analysis

Fig. 1 presents the XRD patterns of both undoped and Cu-doped TiO_2 NPs. The diffraction peaks observed at the crystallographic planes (101), (004), (200), (105), (211), (204), (116), (220), and (215) match closely with the standard anatase phase (JCPDS 84-1286) of TiO_2. Notably, the absence of impurity peaks in the XRD patterns for samples 0.025 M, 0.05 M, 0.075 M, and 0.10 M Cu–TiO_2 confirms that Cu^{2+} ions have been well substituted into the TiO_2 lattice without forming any secondary phases.[20,26] Furthermore, no peaks corresponding to the brookite or rutile phases were detected in any of the prepared samples, indicating that the introduction of Cu does not induce any phase transformation in the TiO_2 structure. A minor displacement of the (101) peak towards reduced 2θ values signifies the effective integration of Cu^{2+} ions into the TiO_2 lattice. The crystallite size was calculated and tabulated in Table 1 using the Scherrer equation.

The XRD analysis reveals that the average crystallite sizes of pure TiO_2 and Cu-doped TiO_2 NPs with varying Cu concentrations (0.025 M, 0.05 M, 0.075 M, and 0.10 M) are approximately 10.9 nm, 10.2 nm, 9.1 nm, 8.3 nm, and 7.9 nm, respectively.[26] A noticeable trend emerges, showing a reduction in the average crystallite size as the Cu concentration increases from 0.025 M to 0.10 M. This indicates a strong dependence of crystallite size on the concentration of Cu doping. When Cu^{2+} ions are introduced into the TiO_2 lattice, they occupy specific lattice sites, leading to changes in the ionic radii of the Cu^{2+} and Ti^{4+} ions. The presence of Cu in the TiO_2 structure restricts the growth of TiO_2 crystallites, particularly up to an optimal doping level. The reduction in grain size is further influenced by Cu atoms at grain boundaries or nanoparticle surfaces.[29] These observations suggest that Cu doping effectively modulates the crystallite size of TiO_2, a behavior also observed in case of other transition metals.[22,29] The variation in crystallite size indicates the successful incorporation of Cu^{2+} ions into the TiO_2.

3.2. SEM-EDS analysis

The surface morphology and elemental composition of the synthesized samples were analyzed using FE-SEM coupled with EDS. Fig. 2 illustrates the SEM images of pure TiO_2 and Cu-doped TiO_2 samples at various Cu concentrations (0.05 M, 0.075 M, and 0.1 M). The SEM images display clear morphological differences between the samples.[26] In the moderately doped samples (0.05 M and 0.075 M), the particles are uniformly distributed, predominantly spherical in shape, and exhibit minimal signs of agglomeration. While, the sample with a higher Cu concentration (0.1 M) shows a more pronounced aggregation, with particles forming

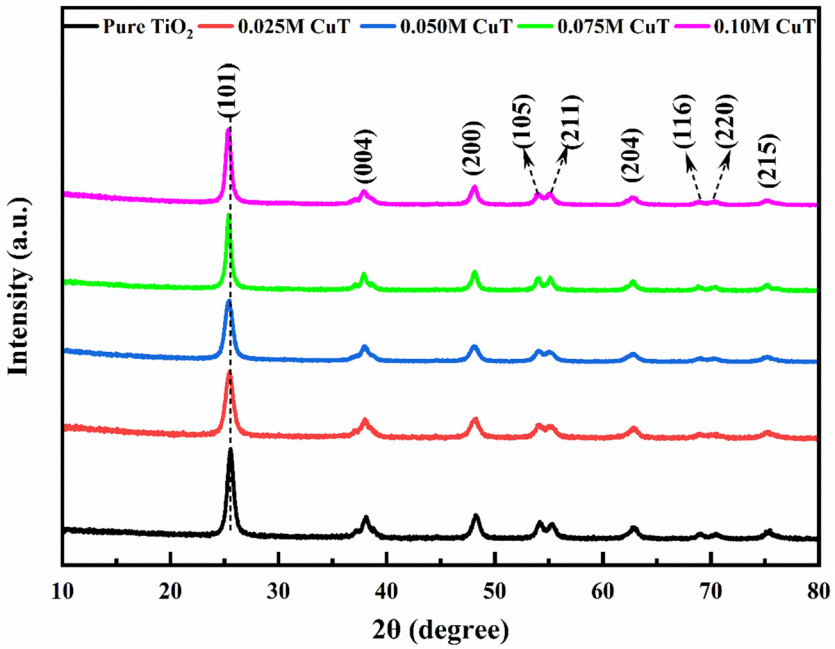

Fig. 1 XRD pattern of pure TiO_2 and various Cu-doped TiO_2 samples.

noticeable clumps. The results highlight how increasing Cu content influences the surface morphology of the NPs, showing significant changes with higher Cu doping levels.[30]

Furthermore, the EDS images and mapping of pure TiO_2 and Cu-doped TiO_2 samples (0.025 M and 0.05 M), shown in Fig. 3, confirm the high purity of the produced nanomaterials. The EDS analysis reveals that the elements present in the samples are in precise stoichiometric ratios, with no detectable impurities or traces of unwanted elements.[30,31] This finding proves that the synthesis method utilized in this work was accurate and reliable, and it also provides strong evidence that the produced nanomaterials are pure and unadulterated.[26]

3.3. HRTEM analysis

In Fig. 4, we have shown the selected area electron diffraction (SAED) patterns, TEM, HRTEM and inverted fast Fourier transform (FFT) images of pure and 0.075 M Cu-doped TiO_2 NPs. Fig. 4(a)–(d) and Fig. 4(e)–(h) respectively display the SAED pattern, TEM, HRTEM and inverted FFT images of pure and 0.075 M Cu-doped TiO_2 NPs. Fig. 4(a) presents the SAED pattern of pure TiO_2 NPs, where distinct concentric rings can be clearly observed, each corresponding to different crystal planes, thereby confirming the polycrystalline nature of the TiO_2 NPs. Similarly, Fig. 4(e) exhibits the same characteristic pattern, reinforcing the polycrystalline nature of 0.075 M Cu-doped TiO_2 NPs. Moreover, the TEM images in Fig. 4(b) and (f) reveal that the NPs are uniformly distributed and exhibit a spherical morphology with limited agglomeration, which supports the findings observed in the FE-SEM analysis.

We further analyzed the HRTEM images of both samples using the FFT and IFFT tools in ImageJ software to determine the interplanar spacing. For the TiO_2 NPs, we applied FFT and IFFT to the most prominent crystalline planes in Fig. 4(c), resulting in an inverted FFT image. From this image, we obtained a profile plot of the crystalline planes and calculated a *d*-spacing value of 0.351 nm, corresponding to the prominent (101) plane of the anatase phase of TiO_2.[23,32] A similar analysis of the 0.075 M Cu-doped TiO_2 sample revealed a *d*-spacing of 0.352 nm, corresponding to the (101) plane of the anatase phase of TiO_2.[32] Additionally, Fig. 4(c) and (g) highlight the ordered structure, along with confirming the polycrystalline nature of both samples.

Table 1 Estimated crystallite sizes, band gap, and dye loading in different samples

Sample	Average crystallite size (nm)	Estimated band gap (eV)	Estimated dye loading (mole cm^{-2})
Pure TiO_2	10.9	3.12	5.44×10^{-8}
0.025 M Cu–TiO_2	10.2	2.96	6.80×10^{-8}
0.050 M Cu–TiO_2	9.1	2.90	8.28×10^{-8}
0.075 M Cu–TiO_2	8.3	2.80	9.94×10^{-8}
0.100 M Cu–TiO_2	7.9	2.71	4.84×10^{-8}

3.4. Raman analysis

Raman spectroscopy was utilized to investigate the localized structural modifications resulting from Cu doping in the synthesized TiO_2 NPs. The Raman spectra of the samples, illustrated in Fig. 5, affirm the existence of the anatase phase of TiO_2, with no signal of Cu or its oxide phases. The prominent peak at 148 cm^{-1} corresponds to the E_g mode of anatase TiO_2, aligns with findings from previous studies.[22,30,33] Additional peaks observed at 198.1 cm^{-1} and 639 cm^{-1}, along with the B1g mode at 399 cm^{-1} and the A1g + B1g mode at 519.46 cm^{-1}, further validating the anatase structure.[26]

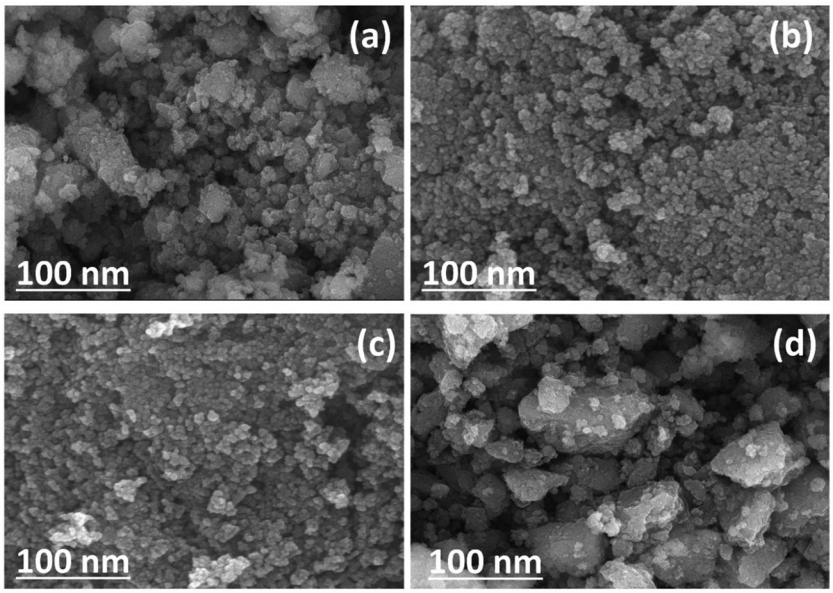

Fig. 2 FE-SEM images for (a) undoped TiO_2, (b) 0.05 M, (c) 0.075 M, and (d) 0.1 M Cu–TiO_2 samples.

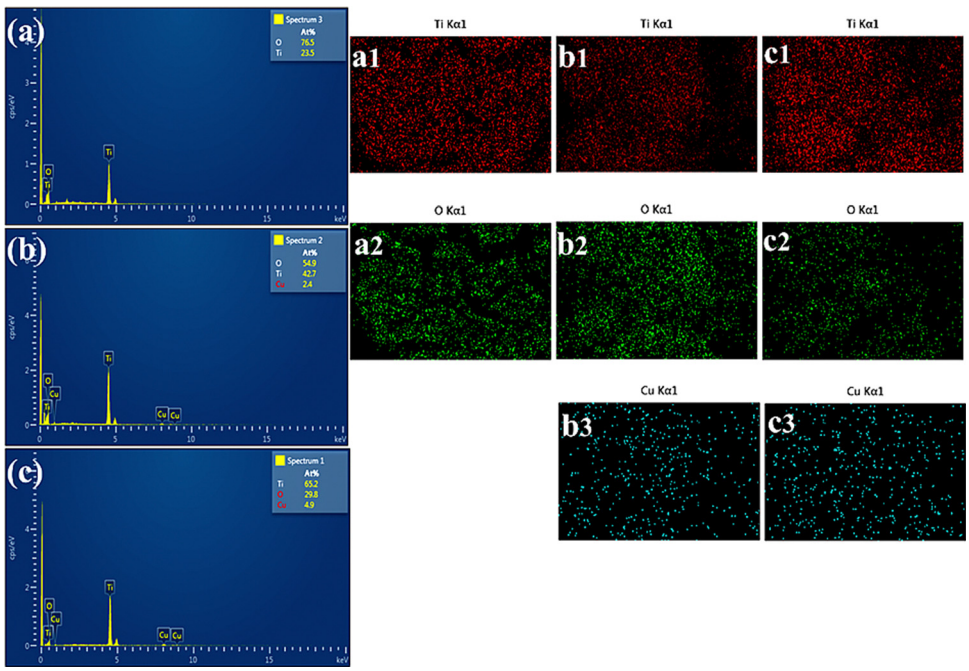

Fig. 3 EDS images and mapping of pure TiO_2 (a)–(a2), 0.025 M Cu–TiO_2 (b)–(b3), and 0.05 M Cu–TiO_2 (c)–(c3) samples.

With increasing Cu doping levels, the Raman spectra exhibit noticeable changes, such as broader peaks and a shift toward higher wavenumbers. These modifications are ascribed to the greater ionic radius of Cu^{2+} (0.73 Å) relative to Ti^{4+} (0.64 Å), resulting in lattice distortion and the formation of oxygen vacancies to preserve charge equilibrium.[26,34] Cu doping disturbs the Ti–O–Ti bonds, resulting in the formation of additional Cu–O–Ti or Cu–O–Cu connections, hence influencing the Raman-active modes. The expansion and displacement of the E_g peak are mainly linked to the vibrations of Cu–O–Cu connections, which diminish in intensity when neighboring oxygen vacancies occur, resulting in lattice contraction and shifts of the peak to higher wavenumbers. The expansion and displacement of the Raman peaks are also influenced by phonon confinement effects and structural defects, such as grain boundaries, as confirmed by XRD analysis.[22,35] These findings offer valuable insights into the structural modifications and vibrational characteristics of Cu-doped TiO_2 NPs, emphasizing

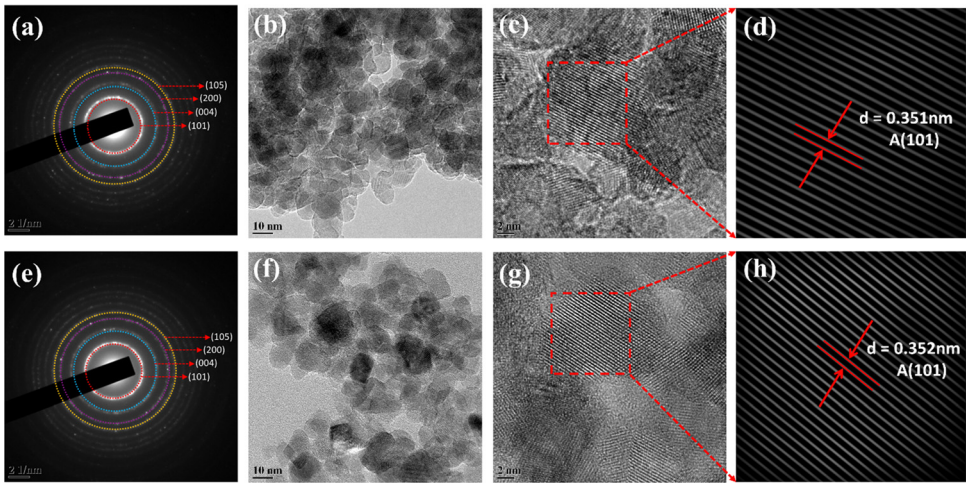

Fig. 4 SAED patterns, TEM, HRTEM and FFT images of (a)–(d) pure TiO_2; and (e)–(h) 0.075 M Cu-doped TiO_2 samples.

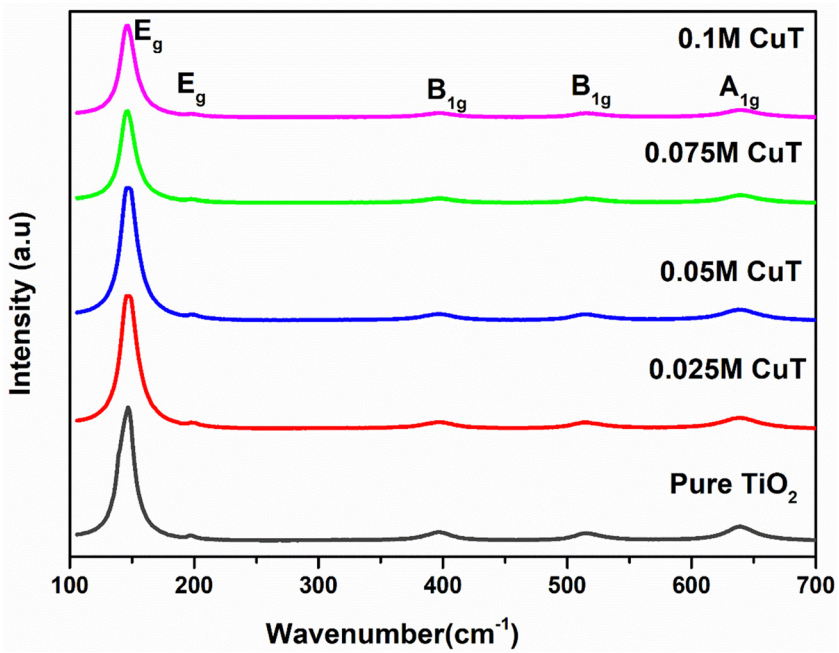

Fig. 5 Raman spectra of pure TiO_2 and various Cu-doped TiO_2 samples.

the influence of Cu incorporation on the local lattice structure and Raman-active vibrational modes of the material.

3.5. UV-Vis analysis

Ultraviolet diffused reflectance spectroscopy (UV-DRS) was employed to analyze Cu-doped TiO_2 NPs. As illustrated in Fig. 6, the reflectance progressively decreases with increasing Cu concentration. This shift in absorption toward the visible spectrum corresponds to electronic transitions from the valence band (VB), primarily composed of O 2p states, to the conduction band (CB), mainly consisting of Ti 3d states. The observed absorption behavior highlights changes in the material's electronic structure, governing the movement of electrons between these energy levels. Furthermore, the UV-vis absorbance spectra of pure and Cu-doped TiO_2 NPs are depicted in Fig. 7(a). In the case of pure TiO_2, the absorbance shows a characteristic absorption edge around 380 nm, corresponding to the intrinsic band gap energy of TiO_2. This absorption in the UV region indicates that pure TiO_2 primarily absorbs ultraviolet light, a property well-known for its photocatalytic activity. A notable redshift in the absorption edge is observed upon doping with Cu, suggesting a reduction in the band gap energy. Fig. 7(b) presents the Kubelka–Munk plots for both pure TiO_2 and Cu-doped TiO_2 NPs, which were used to calculate the band gap energy assuming an indirect electronic transition. The corresponding band gap values are summarized in Table 1,

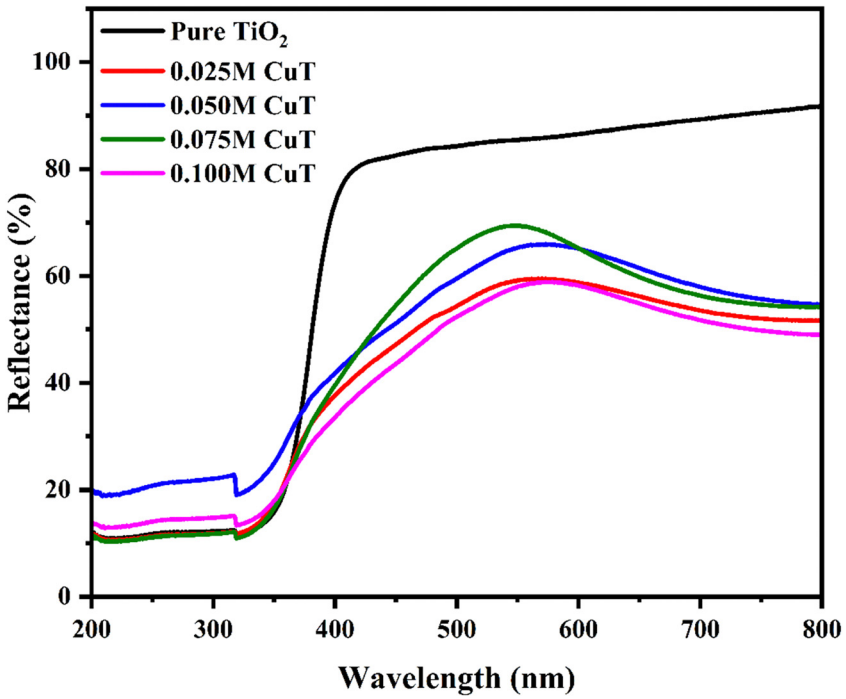

Fig. 6 UV-Vis DRS specta of pure TiO_2 and different Cu-doped TiO_2 samples.

showing that Cu doping leads to a gradual reduction in the band gap. As Cu concentration increases, the band gap of TiO_2 narrows progressively from 3.12 eV for undoped TiO_2 to 2.96 eV (0.025 M Cu), 2.90 eV (0.05 M Cu), 2.80 eV (0.075 M Cu), and 2.71 eV (0.10 M Cu). The slight reduction in the band gap for undoped TiO_2 (3.14 eV as compared to the reported 3.2 eV) can be attributed to the incorporation of carbon during synthesis. In Cu-doped samples, however, the observed band gap reduction is primarily due to the integration of Cu^{2+} ions, which introduce additional electronic states near the conduction band edge and increase impurity levels in the valence band, thereby narrowing the effective band gap.[19,20] This effect is driven by factors including reduced particle size, enhanced crystallinity, and higher carrier concentration, primarily due to oxygen vacancies and metal interstitials. These defects serve as charge carrier generation sites, improving short-circuit current density (J_{SC}) and PCE, as seen in 0.075 M Cu-doped TiO_2 DSSCs. These band gap values align with previous studies on Cu-doped TiO_2 materials, where values of 3.28, 3.19, 3.13, 3.05, and 2.81 eV were reported for pure TiO_2 and varying Cu-doping levels (0.1, 0.5, 1, and 5 wt%).[36] Other studies have reported band gaps of 3.0 eV for 1 wt% Cu, 2.75 eV for Cu/Ti = 0.16 (mol mol^{-1}), and as low as 1.6 eV for 7.5% Cu doping.[37] Further investigation is needed to clarify the solubility limits and incorporation of Cu into the TiO_2 lattice, as current literature presents conflicting views. While some researchers argue that the difference in ionic charge between Cu^{2+} and Ti^{4+} hinders Cu incorporation into the TiO_2 lattice, others provide evidence supporting successful Cu doping within the TiO_2 structure.

In addition, the dye adsorption on TiO_2 film surfaces has been analyzed by determining the dye concentration within the film (Fig. 7c). To measure this, sensitized films are immersed in 1 mM solution of NaOH to desorb the dye from the film's surface.[28,38] The desorbed dye concentration is then quantified using UV-visible spectrophotometry. Table 1 presents the dye concentrations of various TiO_2 films sensitized with anthocyanin dye. The findings reveal that the up to 0.075 M Cu–TiO_2 film exhibited a notable enhancement in dye adsorption compared to other films. However, with further increases in Cu content, dye adsorption declined sharply. This decrease is likely due to reduced nanoparticle size and increased crystallite aggregation, which reduces the films' specific surface area. At higher Cu loading levels, CuO begins to appear on the surfaces of TiO_2 NPs, and the additional Cu species may interact with key functional groups (–OH, $–OCH_3$ and C═O) of the anthocyanin dye rather than binding to the TiO_2 NPs, leading to reduced dye adsorption.[38,39]

3.6. XPS analysis

Analytical tests using X-ray photoelectron spectroscopy (XPS) were performed to determine the chemical composition of pure and Cu-doped TiO_2 NPs. The survey spectrum shown in Fig. 8(a) demonstrates the existence of Cu in the optimized 0.075 M Cu–TiO_2 sample. The core level spectra were analyzed in more detail, uncovering clear peaks corresponding to the titanium (Ti $2p_{1/2}$ and $2p_{3/2}$) and copper (Cu $2p_{1/2}$ and $2p_{3/2}$) levels.[40,41] These peaks are fitted and displayed in Fig. 8(b) and (d). The measured binding energies for the Ti $2p_{1/2}$ and Ti $2p_{3/2}$ peaks were 464.1 and 458.4 eV, respectively. The binding energies of the Cu $2p_{1/2}$ and $2p_{3/2}$ peaks were determined to be 951.93 eV and 932.30 eV, respectively, which aligns with the findings of prior published investigations.[20,22] This observation

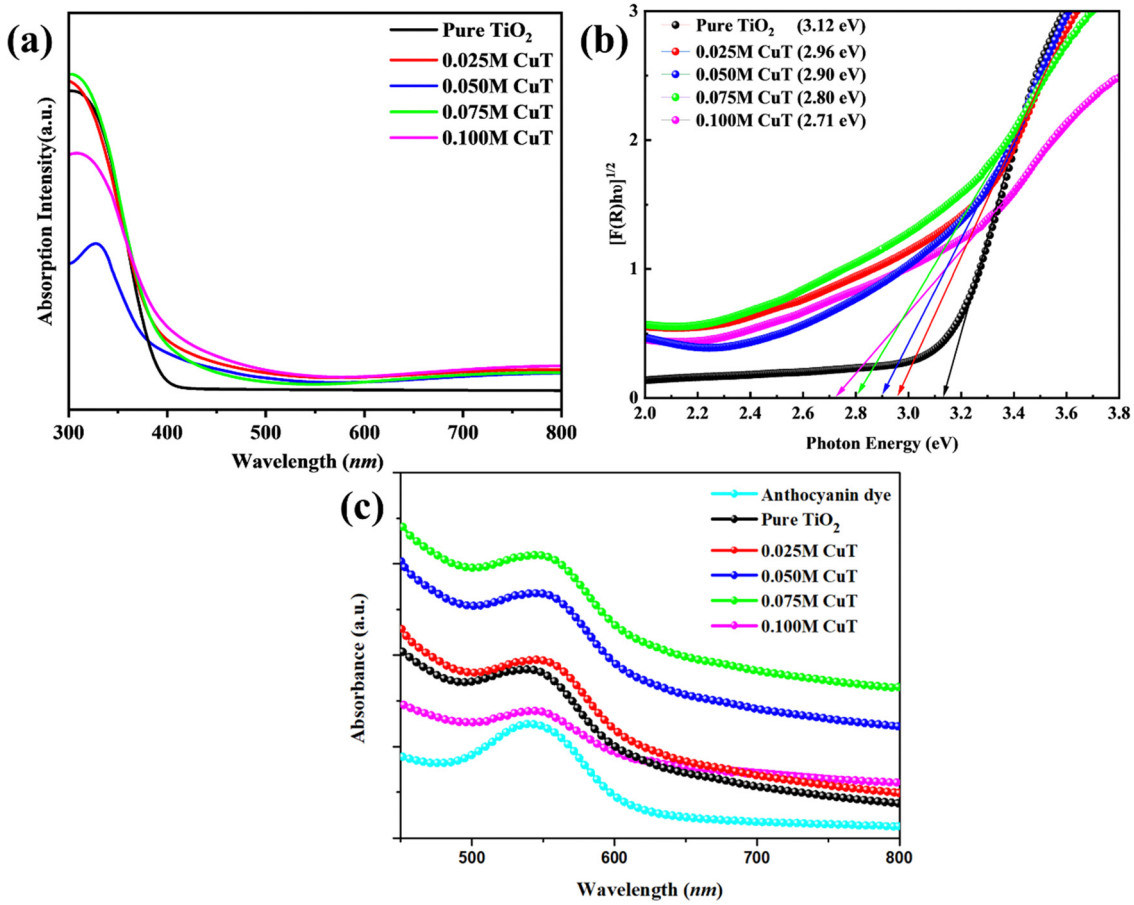

Fig. 7 (a) and (b) UV-Vis absorbance spectra and Tauc plots for undoped TiO_2 and different Cu-doped TiO_2 samples; and (c) absorbance spectra of anthocyanin sensitized various TiO_2 films.

clearly indicates the integration of Cu elements into the composition of the TiO_2 NPs.

Furthermore, the existence of oxygen was verified by the peak detected at 528.8 eV, which corresponds to O 1s (Fig. 8c). Notably, a small variation in the binding energy of titanium atoms was observed, suggesting the replacement of certain Ti^{4+} ions with Cu^{2+} ions at specific locations within the TiO_2 structure.[42] Hence, the XPS analysis provides conclusive proof of Cu doping in the TiO_2 nanostructures, as indicated by the prominent peaks representing Cu and the observed shift in the binding energy of Ti, indicating the integration of Cu ions into the TiO_2 structure. The XPS spectrum for Cu 2p indicates the presence of both Cu^{+} and Cu^{2+} oxidation states in the sample, with higher Cu concentrations in TiO_2 making these states more prominent. Peaks at 934.55 and 953.68 eV correspond to the Cu^{+} state, while those at 932.30 and 951.93 eV are associated with the Cu^{2+} state, as depicted in Fig. 8(d). Additionally, two satellite peaks at 941.8 eV and 943.93 eV observed in the Cu_2–TiO_2 catalyst further confirm the presence of Cu^{2+} species.

3.7. *J–V* analysis

To evaluate the impact of Cu doping on the photovoltaic performance of Cu–TiO_2 nanocomposites, three distinct DSSCs were fabricated using pure TiO_2 and varying compositions of Cu–TiO_2. Fig. 9 presents the current density–voltage (*J–V*) curves for these DSSCs, while Table 2 summarizes key parameters, including open-circuit voltage (V_{OC}), short-circuit current density (J_{SC}), fill factor (FF), and photoconversion efficiency (η). The DSSC based on pure TiO_2 exhibited a PCE of 1.53%, with a J_{SC} of 5.8 mA cm^{-2} and a V_{OC} of 0.6 V. Notably, the incorporation of Cu into the TiO_2 matrix led to a marked enhancement in the photovoltaic performance of the DSSCs.[43,44] The champion DSSC, which included a 0.075 M CuT nanocomposite, demonstrated a significant PCE of 2.61%. This represents a substantial 41% increase compared to the pure TiO_2 equivalent. This enhanced performance is attributed to the reduced band gap of the TiO_2 film, which enables greater light absorption across the visible spectrum, thereby improving light harvesting efficiency.[28]

The addition of Cu dopants had a two-fold impact on the cell performance. Indeed, it resulted in a significant 4% increase in V_{OC} compared to the pure TiO_2 DSSC, suggesting that the presence of Cu caused a reduction in the TiO_2 bandgap.[45] In contrast, an excessive amount of Cu incorporation resulted in the formation of structural flaws, which acted as recombination sites and, therefore, reduced the short circuit current density of the cell compared to moderately doped DSSCs. These findings highlight the collaborative interaction between the inclusion of Cu in TiO_2, which promotes the absorption of dye and

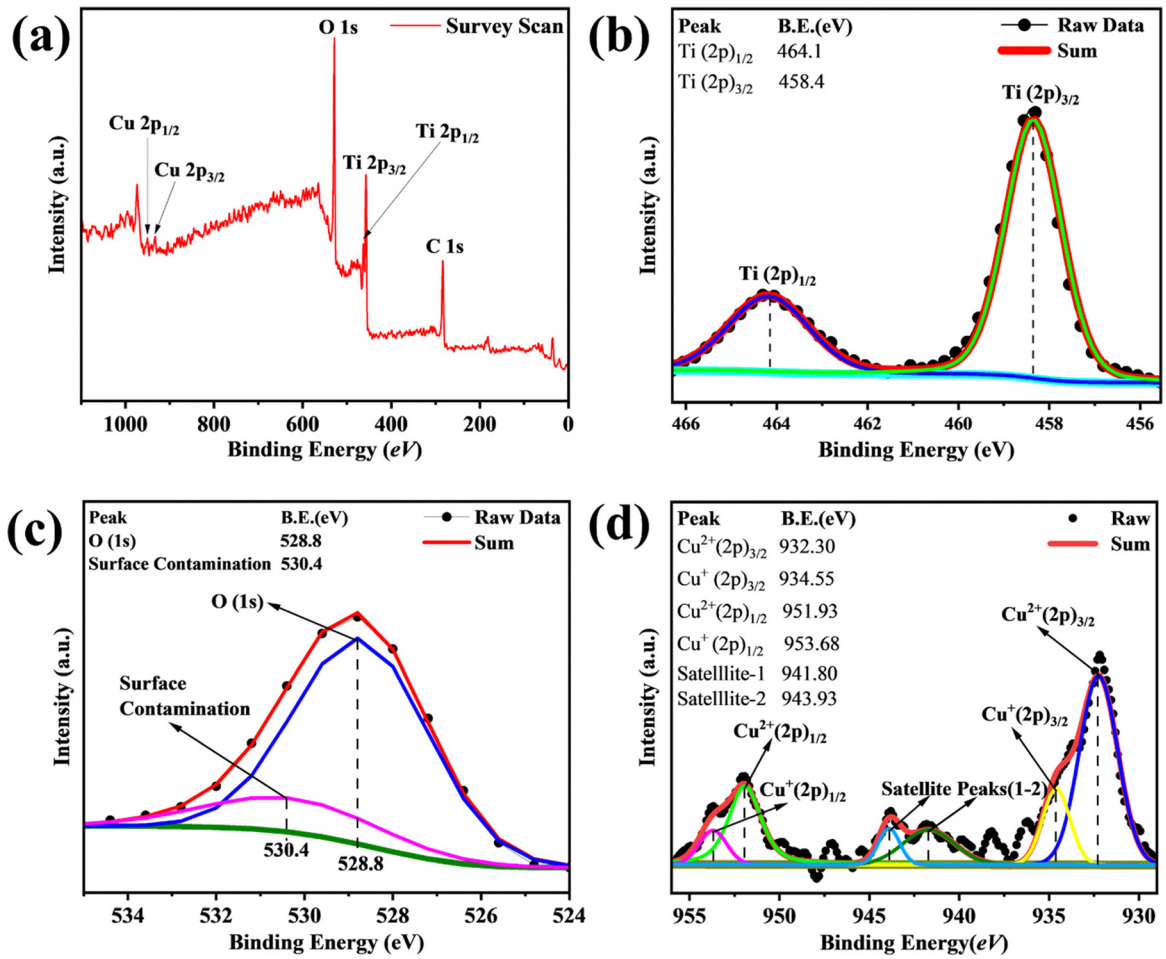

Fig. 8 (a) Survey spectrum of 0.075 M Cu-doped TiO_2 sample; (b) core level spectra of Ti; (c) core level spectra of O; (d) core level spectra of Cu in 0.075 M Cu-doped TiO_2 sample.

separation of charges and consequently improves the J_{SC} and V_{OC}, resulting in a higher PCE. Nevertheless, the detrimental effects of heavy Cu doping were clearly observed in the 0.1 M CuT DSSC. Table 3 presents a comprehensive overview of various studies on Cu-doped TiO_2, summarizing key findings, and performance metrics.

3.8. Incident photon-to-current efficiency (IPCE) analysis

The IPCE of the respective DSSCs, spanning wavelengths from 450 to 800 nm, is depicted in Fig. 10. The highest IPCE value recorded was 68.6% for the 0.075 M CuT photoanodes at 560 nm.[46] In contrast, the maximum IPCE peak values for the 0.050 M CuT, 0.025 M CuT, 0.1 M CuT, and pure TiO_2 photoanodes were 62.3%, 60.9%, 59.1%, and 56.6% respectively. There was a positive correlation between IPCE values and J_{SC}, demonstrating coherence between the J–V study findings and the IPCE analysis. The anthocyanin dye showed absorbance between 400 and 600 nm, corresponding to the maximum IPCE values.[47] The absorption of Cu-doped TiO_2 photoanodes ranged from 450 to 650 nm, corresponding to a bandgap of 2.71–3.12 eV, aligning well with the IPCE study findings. The 0.075 M CuT photoanode-based DSSCs exhibited large IPCE values across a broad spectrum, enhancing light-harvesting capacity due to substantial dye loading and high reflectance.[42] Moreover, the IPCE analysis indicated that DSSCs utilizing Cu-doped TiO_2 photoanodes exhibited a significant red shift toward longer wavelengths, which can be attributed to their enhanced light scattering capabilities.

3.9. Electrochemical impedance spectroscopy (EIS) analysis

The Nyquist plot shown in the Fig. 11, represents the electrochemical impedance spectroscopy analysis of DSSCs based on pure TiO_2 and Cu-doped TiO_2 at different doping concentrations (0.05 M, 0.075 M, and 0.1 M). The semicircle in the Nyquist plot corresponds to the charge transfer resistance (R_{ct}) at the TiO_2/electrolyte interface, which is a crucial parameter in determining the efficiency of DSSCs. A smaller semicircle indicates lower charge transfer resistance and more efficient electron transport, while a larger semicircle signifies higher resistance, leading to increased recombination losses and lower performance.

The DSSC with pure TiO_2 exhibits the smallest semicircle, indicating the lowest charge transfer resistance. However, its relatively small arc suggests limited charge injection and

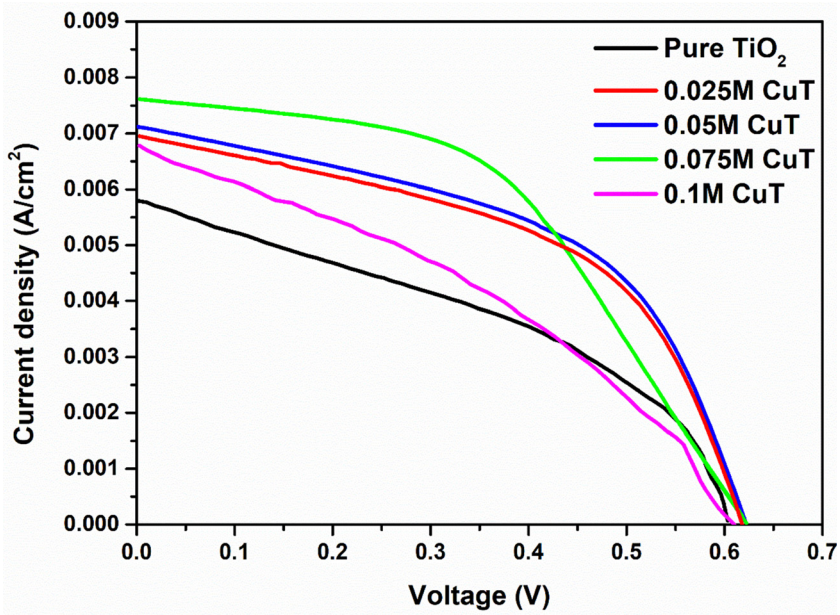

Fig. 9 *J–V* analysis of pure and various Cu-doped TiO_2 DSSCs.

Table 2 Summary of photovoltaic parameters of pure TiO_2 and diverse Cu-doped TiO_2 DSSCs

DSSC composition	J_{SC} (mA cm^{-2})	V_{OC} (mV)	FF	η (%)
Pure TiO_2	5.8	600	0.44	1.53
0.025 M CuT	6.9	620	0.47	2.01
0.05 M CuT	7.2	621	0.49	2.19
0.075 M CuT	7.6	624	0.55	2.61
0.1 M CuT	6.7	610	0.461	1.88

Table 3 Comparison of different studies on Cu-TiO_2 photoanodes with various sensitizers and their photovoltaic parameters

Photoanode	Sensitizer	J_{SC} (mA cm^{-2})	V_{OC} (mV)	FF	η (%)	Ref.
Cu–TiO_2	N719	17.35	730	68	8.9	11
Cu–TiO_2	N719	13.20	762	68.9	6.94	19
Cu–TiO_2	N719	18.8	710	64.2	8.65	20
Cu–TiO_2	N719	7.34	1073	65	5.09	41
Cu–TiO_2	N719	15.1	680	71	7.3	44
Cu,Co/TiO_2	N719	10.78	670	57.4	4.16	45
Cu–TiO_2	Anthocyanin	7.6	624	0.55	2.61	This work

transport, which may result in moderate device efficiency. Upon Cu doping, the semicircle size changes, demonstrating the impact of different doping concentrations on charge transport dynamics. The 0.075 M CuT DSSC exhibits the most optimized response, with a moderate semicircle diameter, suggesting improved charge transfer and reduced recombination losses. This indicates that the introduction of Cu in TiO_2 enhances the electron transport properties and promotes better interaction at the TiO_2/electrolyte interface. The 0.05 M CuT DSSC shows a slightly larger semicircle compared to the 0.075 M CuT DSSC, suggesting that the lower doping concentration is not as effective in reducing charge transfer resistance. However, it still performs better than pure TiO_2 DSSC. In contrast, the 0.1 M CuT DSSC exhibits the largest semicircle among the samples, indicating the highest charge transfer resistance and highest recombination losses. This suggests that excessive Cu doping may introduce structural defects or act as recombination centers, hindering the efficient flow of electrons and reducing DSSC performance.

The observed trend in the Nyquist plot suggests that Cu doping plays a significant role in improving charge transport and reducing recombination losses, but excessive doping can negatively impact performance due to increased defects and charge trapping. The 0.075 M CuT DSSC demonstrates the best balance between enhanced charge transfer and reduced recombination, making it the most optimized configuration among the studied samples.

3.10. Stability test data

The stability of all the DSSC devices was tested under 1 Sun illumination, and the results are shown in Fig. 12. The devices were properly sealed to ensure accurate measurements. Over time, both pure and Cu-doped TiO_2 DSSCs showed a gradual drop in efficiency due to factors like dye degradation, charge recombination, and possible evaporation of the electrolyte. However, the Cu-doped TiO_2 DSSC performed better, maintaining an efficiency of about 1.8% after 30 hours, while the pure TiO_2 DSSC dropped below 0.8%. This shows that adding Cu to TiO_2 improves the stability of the DSSC by enhancing charge transfer and reducing recombination losses. The Cu-doped TiO_2 DSSC lost about 30% of its efficiency over 30 hours, while the pure TiO_2 DSSC lost nearly 50%. This suggests that Cu doping helps extend the lifespan of the DSSC, making it a more reliable material for long-term solar cell applications.

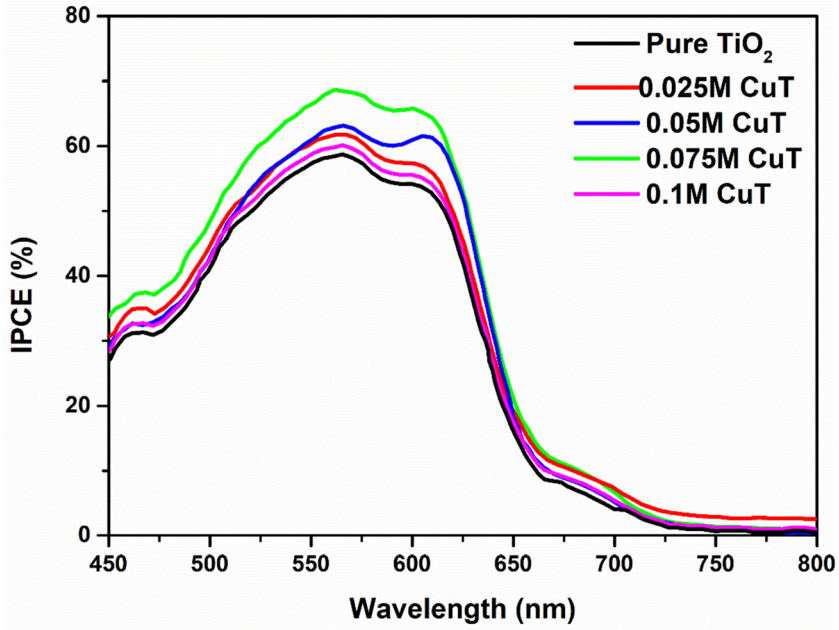

Fig. 10 IPCE spectra of pure and various Cu-doped TiO_2-based DSSCs.

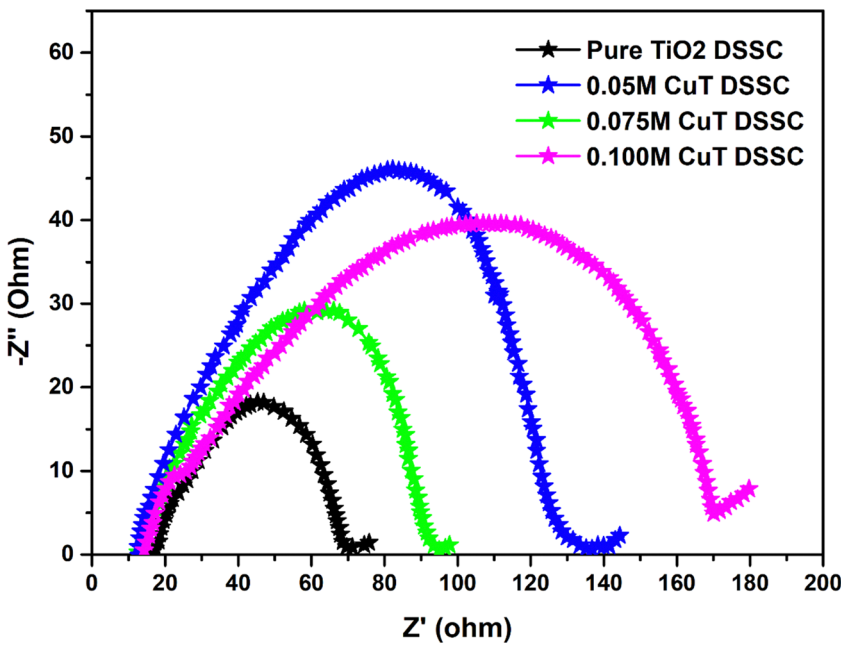

Fig. 11 EIS spectra of pure and various Cu-doped TiO_2-based DSSCs.

4. Conclusions

In conclusion, we have successfully developed a cost-effective DSSC utilizing Cu-doped TiO_2 NPs combined with anthocyanin dyes. To evaluate the impact of these components on DSSC performance, we conducted a series of physicochemical characterization studies and photovoltaic analyses. Our findings indicate that Cu doping significantly reduces photo-charge recombination, while the incorporation of anthocyanin dyes enhances light absorption and energy conversion efficiency. This combination effectively addresses the challenges of low PCE and stability typically associated with DSSCs. Additionally, the use of an economically produced Pt counter electrode enhances charge collection, contributing to overall performance.

This innovative combination of Cu-doped TiO_2 photoanodes, anthocyanin dyes, and Pt counter electrodes has been explored for the first time, resulting in a significant PCE improvement. The simplicity of fabrication, cost-effectiveness,

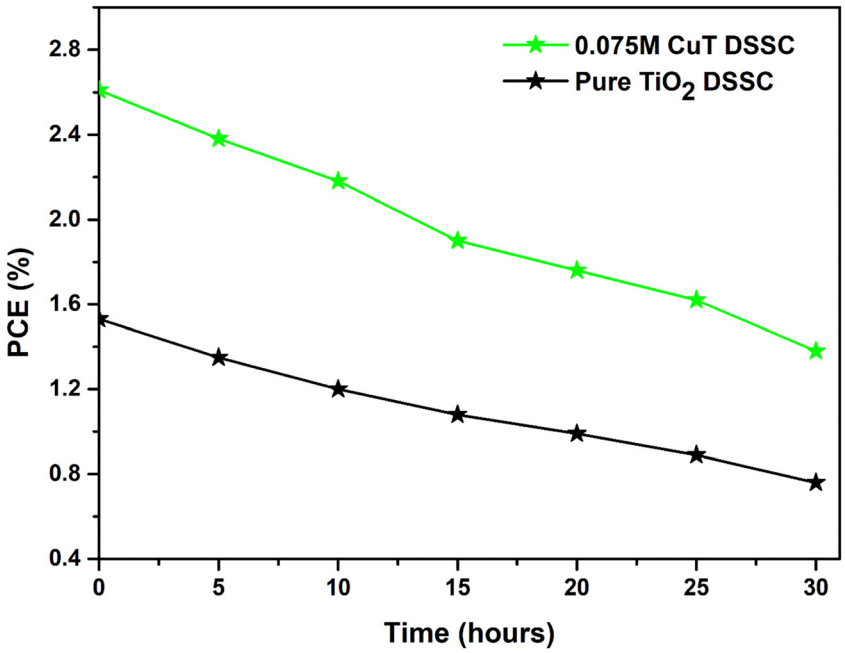

Fig. 12 Stability test graph of the pure TiO_2 DSSC and 0.075 M CuT DSSC.

and eco-friendly nature of this approach, alongside its excellent performance, positions it as a viable solution for commercial production. Notably, a DSSC with a Cu doping concentration of 0.075 M achieved a PCE of 2.61%, a marked increase from the 1.53% efficiency of the undoped variant. In addition, the EIS analysis confirmed that doping with Cu (0.075 M) contributed to the decrease in the electron transport resistance and increase in the recombination resistance of the DSSC. However, it is important to note that higher levels of Cu doping led to decreased adhesion of the TiO_2 layer to the FTO substrates. These advancements indicate that DSSCs incorporating Cu-doped TiO_2 photoanodes and anthocyanin-based photosensitizers have significant potential to revolutionize applications in wearables, low-power internet of things (IoT) devices, and thermochromic technologies.

Data availability

Data will be made available upon reasonable request from the corresponding author.

Conflicts of interest

The authors declare no conflict of interest regarding the publication of this paper.

Acknowledgements

We gratefully acknowledge Medi-Caps University for providing the University Research Fellowship (MU/URF/007) and Seed Money Support (MU/SMPS/No.21). We are also thankful to CMS, KAHE Coimbatore, IIT Indore (MEMS Department), University of Kota, and the UGC-DAE Consortium for Scientific Research, Indore, with special acknowledgement to Dr U. Deshpande for their invaluable laboratory support and insightful discussions, which greatly enhanced this work.

References

1 B. O'Regan and M. Grätzel, A low-cost, high-efficiency solar cell based on dye-sensitized colloidal TiO2 films, *Nature*, 1991, **353**, 737–740, DOI: 10.1038/353737a0.
2 A. Hagfeldt and M. Graetzel, Light-Induced Redox Reactions in Nanocrystalline Systems, *Chem. Rev.*, 1995, **95**, 49–68, DOI: 10.1021/cr00033a003.
3 A. B. Muñoz-García, I. Benesperi, G. Boschloo, J. J. Concepcion, J. H. Delcamp and E. A. Gibson, *et al.*, Dye-sensitized solar cells strike back, *Chem. Soc. Rev.*, 2021, **50**, 12450–12550, DOI: 10.1039/D0CS01336F.
4 A. Sikder, W. Ghann, M. R. Jani, M. T. Islam, S. Ahmed and M. M. Rahman, *et al.*, Characterization and Comparison of DSSCs Fabricated with Black Natural Dyes Extracted from Jamun, Black Plum, and Blackberry, *Energies*, 2023, **16**, 7187, DOI: 10.3390/en16207187.
5 A. Hagfeldt, S. Lindquist and M. Gratzel, Charge carrier separation and charge transport in nanocrystalline junctions, *Sol. Energy Mater. Sol. Cells*, 1994, **32**, 245–257, DOI: 10.1016/0927-0248(94)90262-3.
6 A. S. Teja, A. Srivastava, J. A. K. Satrughna, M. K. Tiwari, A. Kanwade and S. Chand Yadav, *et al.*, Optimal processing methodology for futuristic natural dye-sensitized solar cells and novel applications, *Dyes Pigm.*, 2023, **210**, 110997, DOI: 10.1016/j.dyepig.2022.110997.
7 P. Prakash, B. Janarthanan, M. Ubaidullah, A. M. Al-Enizi, S. F. Shaikh and N. B. Alanazi, *et al.*, Optimization,

fabrication, and characterization of anthocyanin and carotenoid derivatives based dye-sensitized solar cells, *J. King Saud Univ., Sci.*, 2023, **35**, 102625, DOI: **10.1016/j.jksus.2023.102625**.

8 K. Sahu, M. Dhonde and V. V. S. Murty, Efficiency of Solar Cells Based on Natural Dyes with Plasmonic Nanoparticle-Based Photo Anode, *Int. J. Nanosci.*, 2018, **18**, 1850042, DOI: **10.1142/S0219581X18500424**.

9 V. Leela Devi, D. De, P. Kuchhal and R. K. Pachauri, Photovoltaic performance of TiO2 and ZnO nanostructures in anthocyanin dye-sensitized solar cells, *Clean Energy*, 2024, **8**, 144–156, DOI: **10.1093/ce/zkae059**.

10 M. Hussain, T. Jalali, L. Maftoon-Azad and S. Osfouri, Performance Evaluation of Natural Dye-Sensitized Solar Cells: A Comparison of Density Functional Theory and Experimental Data on Chlorophyll, Anthocyanin, and Cocktail Dyes as Sensitizers, *ACS Appl. Electron. Mater.*, 2024, **6**, 1693–1709, DOI: **10.1021/acsaelm.3c01618**.

11 M. Dhonde, K. Sahu and V. V. S. Murty, Cu-doped TiO2 nanoparticles/graphene composites for efficient dye-sensitized solar cells, *Sol. Energy*, 2021, **220**, 418–424, DOI: **10.1016/J.SOLENER.2021.03.072**.

12 M. Dhonde, P. Bhojane, K. Sahu and V. V. S. Murty, Dye-sensitized photoelectrochemical cells in water splitting, *Solar-Driven Green Hydrogen Generation and Storage*, 2023, pp. 157–191, DOI: **10.1016/B978-0-323-99580-1.00005-4**.

13 K. Prajapat, M. Dhonde, K. Sahu, P. Bhojane, V. V. S. Murty and P. M. Shirage, The evolution of organic materials for efficient dye-sensitized solar cells, *J. Photochem. Photobiol., C*, 2023, 55, DOI: **10.1016/j.jphotochemrev.2023.100586**.

14 M. Dhonde, K. Sahu, M. Das, A. Yadav, P. Ghosh and V. V. S. Murty, Review—Recent Advancements in Dye-Sensitized Solar Cells; From Photoelectrode to Counter Electrode, *J. Electrochem. Soc.*, 2022, **169**, 066507, DOI: **10.1149/1945-7111/AC741F**.

15 R. Akilimali, G. S. Selopal, D. Benetti, I. Serrano-Esparza, P. A. Algarabel and J. M. De Teresa, *et al.*, Hybrid TiO2-Graphene nanoribbon photoanodes to improve the photoconversion efficiency of dye sensitized solar cells, *J. Power Sources*, 2018, **396**, 566–573, DOI: **10.1016/J.JPOWSOUR.2018.06.044**.

16 B. Boro, B. Gogoi, B. M. Rajbongshi and A. Ramchiary, Nano-structured TiO2/ZnO nanocomposite for dye-sensitized solar cells application: A review, *Renewable Sustainable Energy Rev.*, 2018, **81**, 2264–2270, DOI: **10.1016/j.rser.2017.06.035**.

17 K. Sahu Dhonde, M. Dhonde and V. V. S. Murty, Novel synergistic combination of Al/N Co-doped TiO2 nanoparticles for highly efficient dye-sensitized solar cells, *Sol. Energy*, 2018, **173**, 551–557, DOI: **10.1016/J.SOLENER.2018.07.091**.

18 K. Sahu, M. Dhonde and V. V. S. Murty, Preparation of copper/TiO2/graphene oxide ternary nanocomposites and their structural, surface morphology, and optical properties, *J. Mater. Sci.: Mater. Electron.*, 2021, **32**, 15971–15980, DOI: **10.1007/S10854-021-06148-2**.

19 K. Sahu, M. Dhonde and V. V. S. Murty, Microwave-assisted hydrothermal synthesis of Cu-doped TiO2 nanoparticles for efficient dye-sensitized solar cell with improved open-circuit voltage, *Int. J. Energy Res.*, 2021, **45**, 5423–5432, DOI: **10.1002/ER.6169**.

20 M. Dhonde, K. Sahu, V. V. S. Murty, S. S. Nemala and P. Bhargava, Surface plasmon resonance effect of Cu nanoparticles in a dye sensitized solar cell, *Electrochim. Acta*, 2017, **249**, 89–95, DOI: **10.1016/J.ELECTACTA.2017.07.187**.

21 M. Dhonde, K. Sahu Dhonde, K. Purohit and V. V. S. Murty, Facile synthesis of Cu/N co-doped TiO2 nanoparticles and their optical and electrical properties, *Indian J. Phys.*, 2019, **93**, 27–32, DOI: **10.1007/s12648-018-1275-4**.

22 T. Raguram and K. S. Rajni, Synthesis and characterisation of Cu-Doped TiO2 nanoparticles for DSSC and photocatalytic applications, *Int. J. Hydrogen Energy*, 2022, **47**, 4674–4689, DOI: **10.1016/J.IJHYDENE.2021.11.113**.

23 N. Prabavathy, R. Balasundaraprabhu, G. Balaji, A. U. Malikaramage, S. Prasanna and K. Sivakumaran, *et al.*, Investigations on the photo catalytic activity of calcium doped TiO2 photo electrode for enhanced efficiency of anthocyanins based dye sensitized solar cells, *J. Photochem. Photobiol., A*, 2019, **377**, 43–57, DOI: **10.1016/J.JPHOTOCHEM.2019.03.038**.

24 K. Omri, I. Najeh, N. Hamdaoui, H. Mansour, M. Madani and S. Mnefgui, Tunability of impedance spectroscopy, electrical conductivity and optical properties of Cu-doped TiO2 nanostructures for optoelectronic device application, *J. Alloys Compd.*, 2024, **1002**, 175252, DOI: **10.1016/J.JALLCOM.2024.175252**.

25 A. Srivastava, J. A. K. Satrughna, M. K. Tiwari, A. Kanwade, S. C. Yadav and K. Bala, *et al.*, Effect of $Ti_{1-x}Fe_xO_2$ photoanodes on the performance of dye-sensitized solar cells utilizing natural betalain pigments extracted from Beta vulgaris (BV), *Energy Adv.*, 2023, **2**, 148–160, DOI: **10.1039/D2YA00197G**.

26 K. Prajapat, U. Mahajan, M. Dhonde, K. Sahu and P. M. Shirage, Synthesis and characterization of TiO2 nanoparticles: Unraveling the influence of copper doping on structural, surface morphology, and optical properties, *Chem. Phys. Impact*, 2024, **8**, 100607, DOI: **10.1016/j.chphi.2024.100607**.

27 U. Mahajan, K. Prajapat, K. Sahu, P. Ghosh, P. M. Shirage and M. Dhonde, Unveiling the impact of TiCl4 surface passivation on dye-sensitized solar cells: enhancing charge transfer kinetics and power conversion efficiency, *J. Mater. Sci.: Mater. Electron.*, 2023, **34**, 2108, DOI: **10.1007/s10854-023-11555-8**.

28 A. Gupta, K. Sahu, M. Dhonde and V. V. S. Murty, Novel synergistic combination of Cu/S co-doped TiO2 nanoparticles incorporated as photoanode in dye sensitized solar cell, *Sol. Energy*, 2020, **203**, 296–303, DOI: **10.1016/J.SOLENER.2020.04.043**.

29 R. D. Çelebi and O. Dayan, Cu-doped TiO2 catalysts for catalytic hydrogenation/degradation of organic compounds in water, *J. Mater. Chem. C*, 2024, **1**, 1–6.

30 Z. U. Rehman, S. Ali, M. Aslam, M. Idrees, A. U. Rehman and J. Iqbal, *et al.*, Optical absorption modeling of bilayer photoanode based on Cu@TiO2 plasmonic dye sensitized solar cells towards photovoltaic applications, *Opt. Quantum Electron.*, 2021, **53**, 371, DOI: **10.1007/s11082-021-03010-x**.

31 J. Manju and S. J. Jawhar, Facile synthesis and characterization of Ti(1−x)CuxO2 nanoparticles for high efficiency dye sensitized solar cell applications, *Opt. Mater.*, 2017, **69**, 119–127, DOI: **10.1016/J.OPTMAT.2017.04.030**.

32 J. O. Olowoyo, M. Kumar, T. Dash, S. Saran, S. Bhandari and U. Kumar, Self-organized copper impregnation and doping in TiO2 with enhanced photocatalytic conversion of H2O and CO2 to fuel, *Int. J. Hydrogen Energy*, 2018, **43**, 19468–19480, DOI: **10.1016/j.ijhydene.2018.08.209**.

33 R. S. Dubey, S. R. Jadkar and A. B. Bhorde, Synthesis and Characterization of Various Doped TiO2 Nanocrystals for Dye-Sensitized Solar Cells, *ACS Omega*, 2021, **6**, 3470–3482, DOI: **10.1021/ACSOMEGA.0C01614/ASSET/IMAGES/LARGE/AO0C01614_0010.JPEG**.

34 K. R. Aneesiya and C. Louis, Localized surface plasmon resonance of Cu-doped ZnO nanostructures and the material's integration in dye sensitized solar cells (DSSCs) enabling high open-circuit potentials, *J. Alloys Compd.*, 2020, **829**, 154497, DOI: **10.1016/J.JALLCOM.2020.154497**.

35 J. Kim, J. Lee, S. Kim, T. Kim, K.-M. Lee and D. Lee, *et al.*, Virucidal activity of Cu-doped TiO2 nanoparticles under visible light illumination: Effect of Cu oxidation state, *J. Hazard. Mater.*, 2024, **465**, 133525, DOI: **10.1016/j.jhazmat.2024.133525**.

36 R. López, R. Gómez and M. E. Llanos, Photophysical and photocatalytic properties of nanosized copper-doped titania sol–gel catalysts, *Catal. Today*, 2009, **148**, 103–108, DOI: **10.1016/J.CATTOD.2009.04.001**.

37 G. Colón, M. Maicu, M. C. Hidalgo and J. A. Navío, Cu-doped TiO2 systems with improved photocatalytic activity, *Appl. Catal., B*, 2006, **67**, 41–51, DOI: **10.1016/J.APCATB.2006.03.019**.

38 J. Y. Park, C. S. Kim, K. Okuyama, H. M. Lee, H. D. Jang and S. E. Lee, *et al.*, Copper and nitrogen doping on TiO2 photoelectrodes and their functions in dye-sensitized solar cells, *J. Power Sources*, 2016, **306**, 764–771, DOI: **10.1016/J.JPOWSOUR.2015.12.087**.

39 R. S. Dubey, S. R. Jadkar and A. B. Bhorde, Synthesis and Characterization of Various Doped TiO2 Nanocrystals for Dye-Sensitized Solar Cells, *ACS Omega*, 2021, **6**, 3470–3482, DOI: **10.1021/ACSOMEGA.0C01614**.

40 L. Zhou, L. Wei, Y. Yang, X. Xia, P. Wang and J. Yu, *et al.*, Improved performance of dye sensitized solar cells using Cu-doped TiO2 as photoanode materials: Band edge movement study by spectroelectrochemistry, *Chem. Phys.*, 2016, **475**, 1–8, DOI: **10.1016/J.CHEMPHYS.2016.05.018**.

41 B. Ünlü and M. Özacar, Effect of Cu and Mn amounts doped to TiO2 on the performance of DSSCs, *Sol. Energy*, 2020, **196**, 448–456, DOI: **10.1016/j.solener.2019.12.043**.

42 A. Zatirostami, A dramatic improvement in the efficiency of TiO2-based DSSCs by simultaneous incorporation of Cu and Se into its lattice, *Opt. Mater.*, 2021, **117**, 111110, DOI: **10.1016/J.OPTMAT.2021.111110**.

43 A. Bartkowiak, O. Korolevych, G. L. Chiarello, M. Makowska-Janusik and M. Zalas, Experimental and theoretical insight into DSSCs mechanism influenced by different doping metal ions, *Appl. Surf. Sci.*, 2022, **597**, 153607, DOI: **10.1016/j.apsusc.2022.153607**.

44 V. Bhullar and A. Mahajan, Cu implanted TiO2 based dye sensitized solar cells: Unraveling the effect of doping mechanism and type of metal ion on the photovoltaic properties, *Sol. Energy*, 2023, **254**, 8–14, DOI: **10.1016/j.solener.2023.03.002**.

45 J. H. Bae, H. J. Jeon, S. H. Cho, Y. B. Cho, S. E. Lee and T. O. Kim, Efficiency improvement of dye-sensitized solar cells using Cu,Co/TiO2 photoelectrodes doped by applying ultrasonic treatment, *Appl. Surf. Sci.*, 2023, **621**, 156823, DOI: **10.1016/J.APSUSC.2023.156823**.

46 S. Shakir, Z. S. Khan, A. Ali, N. Akbar and W. Musthaq, Development of copper doped titania based photoanode and its performance for dye sensitized solar cell applications, *J. Alloys Compd.*, 2015, **652**, 331–340, DOI: **10.1016/J.JALLCOM.2015.08.243**.

47 H. Esgin, Y. Caglar and M. Caglar, Photovoltaic performance and physical characterization of Cu doped ZnO nanopowders as photoanode for DSSC, *J. Alloys Compd.*, 2022, **890**, 161848, DOI: **10.1016/J.JALLCOM.2021.161848**.